European Polymer Journal 117 (2019) 28–37

Contents lists available at ScienceDirect

European Polymer Journal

journal homepage: www.elsevier.com/locate/europolj

Polyaniline-polycaprolactone blended nanofibers for neural cell culture

Fábio F.F. Garrudo[a,b,c], Caitlyn A. Chapman[a], Pauline R. Hoffman[a], Ranodhi W. Udangawa[a], João C. Silva[a,b,c], Paiyz E. Mikael[a], Carlos A.V. Rodrigues[b,c], Joaquim M.S. Cabral[b,c], Jorge M.F. Morgado[d], Frederico C. Ferreira[b,c], Robert J. Linhardt[a,*]

[a] Center for Biotechnology & Interdisciplinary Studies, Department of Chemistry & Chemical Biology, Rensselaer Polytechnic Institute, Biotechnology Center 4005, Troy, NY 12180, USA

[b] Department of Bioengineering and iBB – Institute for Bioengineering and Biosciences, Instituto Superior Técnico, Universidade de Lisboa, Lisboa, Av. Rovisco Pais, Lisboa 1049-001, Portugal

[c] The Discoveries Centre for Regenerative and Precision Medicine, Lisbon Campus, Instituto Superior Técnico, Universidade de Lisboa, Av. Rovisco Pais, Lisboa 1049-001, Portugal

[d] Department of Bioengineering and Instituto de Telecomunicações, Instituto Superior Técnico, Universidade de Lisboa, 1049-001 Lisboa, Portugal

ARTICLE INFO

Keywords:
Polyaniline
Electrospinning
Electroconductive nanofibers
Neural stem cells
Neural tissue engineering

ABSTRACT

Neurodegenerative diseases compromise the quality of life of increasing numbers of the world's aging population. While diagnosis is possible, no effective treatments are available. Using both tissue engineering and nanomedicine approaches, it is possible to develop systems appropriated for cell transplantation. Culturing neural stem cells (NSCs) on conductive polymers promotes their differentiation yield. The study herein aims at optimizing and characterizing NSC-compatible, electrically conductive poly(capro-ε-lactone) (PCL)-polyaniline (PANI) electrospun scaffolds for neural tissue engineering applications. Furthermore, the optimal PANI to PCL ratio required for ideal electroconductivity properties is still not well understood. The obtained fibers were characterized by FTIR, TGA and DSC, and their material's mechanical properties and electroconductivity, were investigated. For the first time, PCL-PANI fiber's biocompatibility was assessed in NSCs; cell adhesion, growth rate and morphology were evaluated and correlated with the material's physico-chemical properties. All the samples tested were able to support neural stem cell growth without any major changes on the cell's typical morphology. We were also successfully able to produce electrically conductive nanofibers with conductivities above of biological fluids (7.7×10^{-2} S/cm vs 1.0×10^{-2} S/cm), making these ideal candidates for in vitro neural differentiation studies under electrical stimulation. Overall, this study provides valuable knowledge to improve future, in vitro models for drug testing and tissue engineering applications.

1. Introduction

Neurodegenerative diseases compromise the health of increasing numbers of the world's aging population. They are caused by a progressive loss of the patient's brain cells, and the signs vary based on the disease and the affected area of the brain. Most commonly essential brain functions gradually disappear, including memory, judgement, and movement control. Alzheimer's disease (AD), the most common cause of all dementia (60–80%), is estimated to affect 24 million people globally, with an incidence of 0.6% for patients of 65–69 years old and 6% for 85 years old patients [1] Parkinson's disease (PD), the second most common neurodegenerative disease, has comparatively lower incidence (8–18 cases per 100,000 annually) and is observed in 1% of 60-year-old patients and in about 3% of patients older than 80 years of age. Life span after onset of PD is just 15 years [1]. While diagnosis is possible, no effective cures are available for these diseases and treatments available are only palliative. Although some risk factors, especially for AD, have been extensively reported, *i.e.*, old age, genetics, cerebrovascular disease, and other conditions such as obesity, diabetes and smoking, the etiological uncertainty of the diseases remains a challenge [1].

Replenishing neurons is the ultimate therapy to cure these otherwise progressive, debilitative and fatal neurodegenerative diseases. Cell therapy, with neural stem cells (NSCs) or mesenchymal stem cells (MSCs), has potential for effectively treating neurodegenerative diseases, either by replenishing the cell pool or through the secretion of paracrine factors [2–6]. However, these therapies do not take into account that these diseases: (1) are multifactorial; (2) negatively impact

* Corresponding author.
E-mail address: linhar@rpi.edu (R.J. Linhardt).

https://doi.org/10.1016/j.eurpolymj.2019.04.048
Received 17 February 2019; Received in revised form 25 April 2019; Accepted 28 April 2019
Available online 29 April 2019

the brain ECM; and, therefore, (3) hamper any chances for survival and/or an optimal differentiation of NSCs into fully mature and functional neurons and glial cells [7]. Carradori and coworkers review some of these factors and remind us that no clinical trial using stem cells for neurodegenerative diseases has yet reached phase III studies [5].

Tissue engineering focuses on the development of tissue and organ substitutes, restoring or augmenting their structure and functions [8]. A potential combination between tissue engineering, nanotechnology and material science is critical for the development of successful tissue engineering strategies targeting neurodegenerative diseases [5]. Particularly important is the development and optimization of biomaterials and nanostructured scaffolds that can support NSCs growth, differentiation and maturation. Such biomaterials require the optimization of diverse physical properties, including mechanical properties, chemical cues, and electroconductivity, to modulate cell behavior and mimic the target tissue microenvironment [9,10]. One important cue in engineering neural tissue replacements is the direct electrical stimulation of cells. Electrical stimulation can not only enhance proliferation but also promote migration and differentiation of various cell types, including cardiomyocytes and neural cells [9,11–13]. *In vitro*, NSCs exposed to electric fields adopt a more elongated morphology, [12] resulting in an increased number of neurites, [14,15] and expression of higher level of neuron specific proteins (i.e., Tuj1, MAP2) [9,11]. The *in vivo* use of electricity to directly stimulate the entorhinal and hippocampal regions (deep brain stimulation) can also impact memory and learning [16–18].

Conductive polymers have been shown to be capable of sustaining cell growth [19] and conduct electric stimuli to cultured cells. Even in the absence of electrical stimulation they can slightly improve NSC differentiation [9,20]. When used for neural tissue engineered scaffolds, conductive polymers can enable direct and electrically tunable cell stimulation, while exhibiting better mechanical properties than metallic-derived biomaterials [12]. In addition, the easy fabrication and processing of conductive polymers into any three-dimensional (3D) structure that suits the requirements of the targeted tissue make these materials ideal candidates for potential therapy in neurodegenerative diseases [21,22].

One particularly useful conductive polymer is poly(aniline) (PANI) [23] When doped with camphorsulfonic acid (CSA), this polymer undergoes a change in its resonance structure, switching from the quinoid-rich, emeraldine base (blue) form to a benzene-rich, emeraldine salt (green) form, making it more conductive [19,24,25]. PANI was proved to be biocompatible [26,27] and has been used in the production of films, [19,28] electrospun fibers [14,29] and hydrogels [30,31] for cell culture applications. Previous studies have also shown the potential application of PANI-poly(caprolactone) (PCL) blended fibers as gas sensors [32] and as scaffolds for myoblasts and HUVECs [33,34]. The blending of PANI with PCL also holds promise in creating a biocompatible and electroconductive scaffold for neural tissue engineering. However, no studies have yet focused on using such blends for culturing NSCs.

Furthermore, the optimal PANI to PCL ratio required for ideal electroconductivity properties is still not well understood. The present study aims at optimizing and characterizing NSC-compatible, electrically conductive PCL-PANI electrospun scaffolds, for applications in neural tissue engineering. This platform will potentially be useful for: (1) building in vitro platforms for drug screening and disease models; (2) serving as an interface for deep-brain electrodes; and (3) allowing the direct transplantation of fully grown and functional neurons into patients' brains.

2. Materials and methods

2.1. Materials

PANI, of molecular weight (MW) 100,000 Da, CSA (98% purity), 2,2,2-trifluoroethanol (TFE), poly(caprolactone) MW 80,000, poly(L-ornithine hydrobromide) MW 30,000–70,000, glucose, human recombinant insulin, 2-(4-amidinophenyl)-6-indolecarbamidine dihydrochloride (DAPI), phalloidin–tetramethylrhodamine B isothiocyanate and osmium tetroxide (4% in H_2O) were purchased from Sigma (St. Louis, MO). Dulbecco's phosphate buffer saline (DPBS), Dulbecco's Modified Eagle's Medium (DMEM-F12 + glutamax (1X)), N2-supplement (100X), pen-strep mixture (penicillin 10,000 units mL^{-1}, streptomycin 10,000 μg mL^{-1}) human recombinant epidermal growth factor (EGF), human recombinant fibroblast growth factor 2 (FGF-2), B27-supplement (50X), reazurin (Alamar Blue® cell viability reagent) and triton-x-100 (Surfact-Amps®, 10% in water) were obtained from Thermofisher. Ultra-low attachment 24-well plates (flat bottom) were obtained from Corning. Medical glue (silastic® medical adhesive silicone type A) was obtained from Biesterfeld Spezialchemie Ibérica, SL. Paraformaldehyde (PFA, 4% in phosphate buffered saline (PBS), ChemCruz) was obtained from Santa Cruz Biotechnology. Normal goat serum (10%) was obtained from Life Technologies. A frozen stock of ReN-VM cells (Millipore) was used in these studies.

2.2. PCL-PANI solution preparation

The various PCL-PANI/CSA, or simply PCL-PANI, solutions were prepared by adding PANI and CSA in ratio of 0.78 g to 1 g respectively following literature reports. [19] Doping occurred upon dissolution of the two compounds in TFE, and the obtained solutions were stirred for 24 h until the color changed from blue to green. PCL was then added to the resulting mixture. Eight different solutions of PCL-PANI were prepared and identified by the PCL:PANI weight ratio (Table 1).

2.3. Electrospinning

The prepared PCL-PANI solutions (Table 1) were electrospun using a spinneret system (MECC, Ogori, Fukuoka, Japan) and a 23G needle (0.635 mm of internal diameter) under the following conditions: voltage of 15 kV, flow rate at 1.0 mL h^{-1}, distance from needle to collector of 15 cm, temperature of 21 °C, relative humidity of 20%. Samples were collected on a static copper collector, and then dried under vacuum before being analyzed.

2.4. Physical characterization of the obtained fiber mats

2.4.1. Fiber mats morphology and fiber diameter

The morphology of the fiber mats obtained was evaluated using Scanning Electron Microscopy (SEM) (Carl Zeiss Supra 55 FESEM) at 1 kV, IL detector, after coating with a thin platinum layer. Fiber diameter was evaluated using SEM images. A total of 100 individual fibers (five images with 20 fibers/image) for each combination were analyzed

Table 1
Identification and composition of the solutions used in the fiber's preparation and corresponding fiber's diameters. Results presented as mean ± sd.

Sample	PANI (mg)	CSA (mg)	PCL (g)	TFE (mL)	Fiber diameters (nm)
88:12	68	87	0.5	10	96 ± 29
91:9	68	87	0.7	10	268 ± 42
93:7	68	87	0.9	10	276 ± 82
94:6	68	87	1.1	10	258 ± 72
95:5	68	87	1.3	10	273 ± 93
96.25:3.75	51	65	1.3	10	348 ± 124
97.5:2.5	33	43	1.3	10	334 ± 154
98.75:1.25	16	21	1.3	10	333 ± 119
PCL 5%	0	0	0.5	10	87 ± 29
PCL 7%	0	0	0.7	10	161 ± 50
PCL 9%	0	0	0.9	10	228 ± 73
PCL 11%	0	0	1.1	10	320 ± 79
PCL 13%	0	0	1.3	10	561 ± 187

using NIH ImageJ software (National Institute of Health, MD, USA). The diameters obtained were averaged and the histograms were plotted using Microsoft Excel.

2.4.2. Attenuated total reflectance–fourier transform infra-red spectroscopy (ATR-FTIR)

A profile of the fiber mat (5 × 2 cm^2) was obtained by FTIR (Perkin Elmer Spectrum One FT-IR Spectrophotometer) using the ATR module. Transmittance spectra were obtained over the region from 650 to 4000 cm^{-1} at room temperature and recorded with an accumulation of 32 scans and a resolution of 4 cm^{-1}.

2.4.3. Thermogravimetric analysis (TGA)

Thermal decomposition of the fiber mats was determined, under a nitrogen atmosphere, using a computer-controlled TA instrument (TGA Q5, New Castle, DE, USA). Samples were heated in alumina crucibles, from 50 °C to 600 °C at a constant heating rate of 1.5 °C min^{-1}. Profiles of mass loss as a function of temperature were obtained and evaluated using TA Universal Analysis 2000 software (Version 4.5A, TA Instruments). The onset temperature of degradation and corresponding mass loss were calculated for each sample using first and second derivatives.

2.4.4. Differential scanning calorimetry (DSC)

The thermal properties of PCL-PANI fibers were determined using a differential scanning calorimeter (DSC) 8500 (Perkin-Elmer). Pre-weighed fibermats were sealed in aluminum pans and heated at 10 °C min^{-1} to 100 °C to ensure even spreading in the pan. After this the samples were subjected to one heating and cooling cycle each between −80 and 100 °C at 1.5 °C min^{-1} under a nitrogen atmosphere. Crystallization, melting and glass-transition temperatures, along with their respective enthalpies, were calculated using TA Universal Analysis 2000 software (Version 4.5A, TA Instruments).

2.4.5. Electroconductivity measurements

Electrospun fiber mats were coated with four 50 nm thick gold strips, using a Temescal e-beam evaporator, to improve electrical contact. The electroconductivity was measured using the 4-probe method on a probe station (Suss Manual 4 Probe Station coupled to Keithley 4200 IV/CV meter). Each mat was measured in 5 different spots, and electroconductivity was averaged from 3 mats. The thickness of the mats was measured using a Dektak 8 Profilometer at 3 mg, 111 μm s^{-1}.

2.4.6. Mechanical tests

A uniaxial tensile test was performed on the electrospun mats using an Instron 5800 (Plansee, Franklin, MA) load frame with a 10 N load cell. Specimens were cut to a rectangular shape (40 mm × 15 mm, n = 5) and the crosshead speed was set constant at 10 mm min^{-1} during the uniaxial test. Young's modulus was calculated from the 0–15% strain linear region in the stress-strain curve and the ultimate tensile strength (UTS) and maximum extension were measured from the highest peak of the stress-strain curve.

2.5. Biocompatibility assessment

2.5.1. ReN-VM cell culture conditions

In this study the human-derived cell line ReN-VM, NSCs immortalized through the transfection of c-myc, is used due to its ease of cell culturing and ability to differentiate into mature neural cells [35].

ReN-VM cells were grown on poly-ornithine (20 μg mL^{-1}) and laminin (10 μg mL^{-1}) coated plates in N2 media, composed of DMEM/F12 with N2 supplement (1:100), additional glucose (1.6 g mL^{-1}), insulin (20 μg mL^{-1}) and pen-strep (1:100), supplemented with EGF (20 ng mL^{-1}), FGF-2 (20 ng mL^{-1}) and B27 (10 μL mL^{-1}), at 37 °C and 5% CO_2.

2.5.2. ReN-VM cell proliferation assay and kinetic data calculation

Electrospun fiber mats, immobilized on glass coverslips with medical glue, were firstly UV sterilized for 1.5 h per scaffold side and treated with 1% pen-strep solution in PBS, for 3 h. They were then coated with poly-ornithine and laminin before being seeded with ReN-VM cells (P10) at 20,000 cells cm^{-2}. Supplemented N2 media was added 1 h after seeding (37 °C and 5% CO_2) to promote initial cell attachment. Media was exchanged at day 1, when cell adhesion was calculated, and then every two days thereafter until the end of the experiment. Cellular metabolic activity was assessed using Alamar Blue® at days 1, 3, 5 and 7. Cell number was determined using a calibration curve. Cell adhesion (Eq. (1)), growth rate, (Eq. (2)) and duplication time (Eq. (3)) were calculated using the following formula:

$$Cell\ \ adhesion\ \ at\ \ day\ \ 1 = (cells\ \ at\ \ day\ \ 1)/(seeded\ \ cells) \quad (1)$$

$$Growth\ \ rate = [ln(cells\ \ day\ 7) - ln(cells\ \ day\ \ 3)]/total\ \ time \quad (2)$$

$$Doubling\ \ time = ln(2)/growth\ \ rate\ (h^{-1}) \quad (3)$$

2.5.3. Confocal imaging

Cells at day 7 were fixed in PFA 4% for 10 min, washed with DPBS twice and then permeabilized with staining solution (goat serum 5% and Triton-x-100 0.1% in DPBS) for 15 min at RT. Phalloidin-Rhodamine (0.5 mg mL^{-1}) and DAPI (1 mg mL^{-1}) staining was performed with staining solution for 45 min and 5 min, respectively. Cells were then washed and kept in DPBS and imaged using a confocal microscope (Zeiss LSM 510META Spectral Confocal). Fixed cells were also treated with osmium tetroxide 1% for 30 min, dried using a critical point dryer (Supercritical automegasamdri 915B, purge at 3), coated with platinum and imaged using SEM (Carl Zeiss Supra 55 FESEM).

2.6. Statistical analysis

All data are presented as mean values ± standard deviations (SD). Statistical analysis was performed using Microsoft Excel. Significant differences between groups were measured using ANOVA test, followed by post-hoc analysis and Bonferroni correction. $p < 0.05$ was considered statistically significant.

3. Results

3.1. Average fiber diameters and histograms

Electrospun PCL-PANI fibers were easily obtained. SEM images of PCL-PANI fibers and their corresponding diameter distribution histograms are shown in Figs. 1 **and S1**. The diameters are within the nanoscale range (Table 1). With the exception of samples 91:9 and 88:12, the addition of PANI:CSA impacted the overall fiber diameter in a statistically significant way when compared to pure PCL fibers. When considering samples 95:5, 96.25:3.75, 97.5:2.5, 98.75:1.25, only 95:5 (273 ± 93 nm) was statistically different from the others. For samples 95:5, 94:6, 93:7, 91:9 and 88:12, where PANI:CSA amount was kept constant but PCL was varied, we found that 91:1 (268 ± 42 nm) and 88:12 (96 ± 29 nm) were each significantly different from the others.

3.2. ATR-FTIR

FTIR spectra for all the fiber blends and standards (PCL 13%, PANI:CSA) demonstrated that both PCL and PANI polymers were blended within the fibers. PCL peaks corresponding to asymmetric/symmetric CH_2 bands (2866 cm^{-1} and 2943 cm^{-1}), carbonyl groups (1727 cm^{-1}) and the fingerprint region (1100–1400 cm^{-1}) could be identified in both PCL and PCL-PANI fibers (Fig. 2**A**). The three characteristic amine peaks in the PANI:CSA standard at 652 cm^{-1}, 830 cm^{-1}, and 946 cm^{-1} were assigned to N−H bending, 3300 cm^{-1}

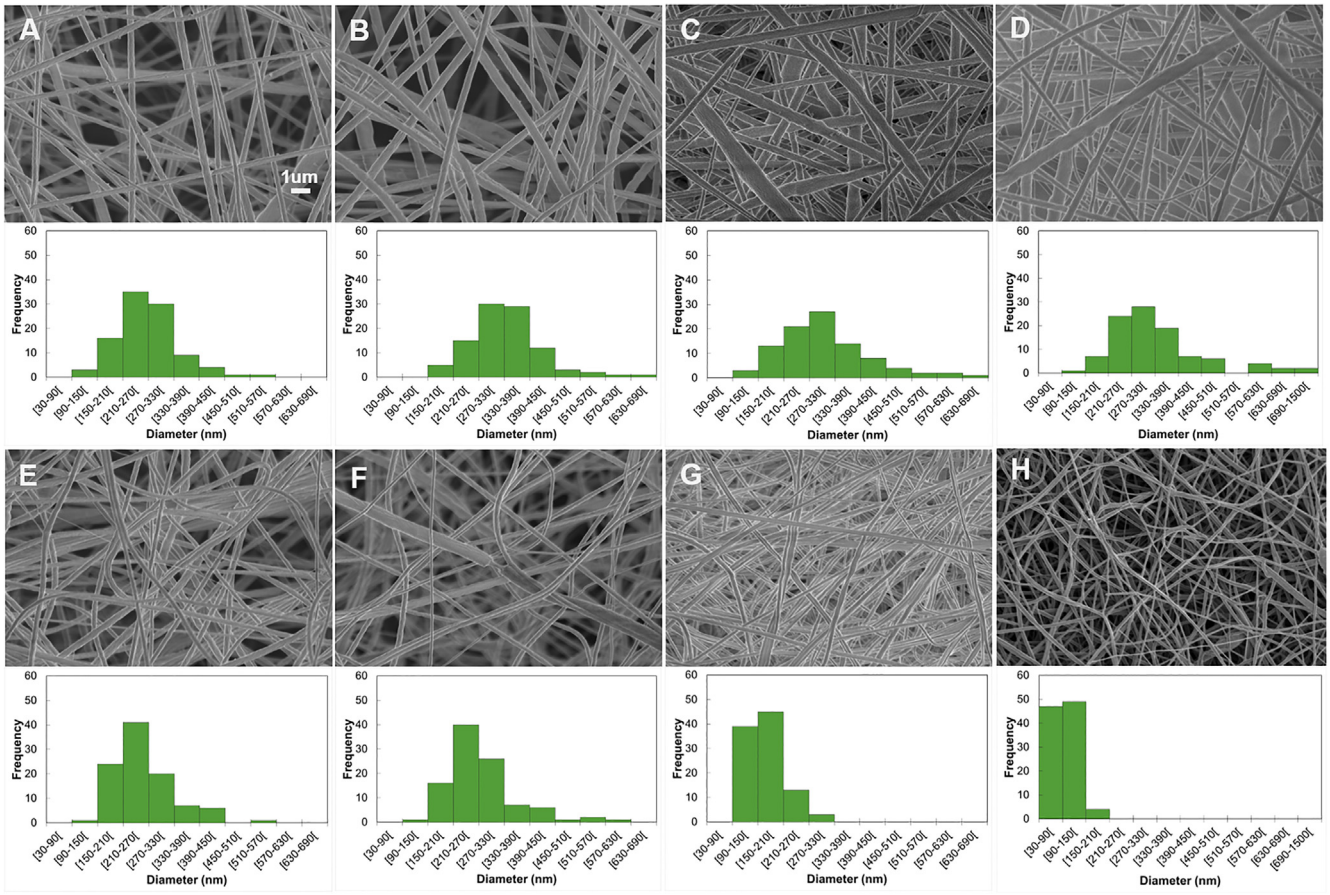

Fig. 1. SEM images (25,000X) and diameter histograms of PCL-PANI electrospun fibers (**A**) 95:5, (**B**) 96.25:3.75, (**C**) 97.5:2.5, (**D**) 98.75:1.25, (**E**) 94:6, (**F**) 93:7, (**G**) 91:9 and (**H**) 88:12. Scale bar 1 μm.

was assigned to N—H stretching but these peaks were not identified in the blended fibers. The peak at 1412 cm^{-1} was assigned to the aromatic ring. New peaks, some of low intensity, were also identified in PCL-PANI fibers, corresponding to the *para*-substituted benzene (794 cm^{-1}) (Fig. 2**C**) and quinoid (1554 cm^{-1}) rings (Fig. 2**B**), nitrile (2336 cm^{-1}), secondary amine (3455 cm^{-1}) and alcohol (3728 cm^{-1}), present in PANI:CSA. These last four peaks showed very weak intensities. Overall, all the PCL-PANI samples have similar spectra, and peaks from both

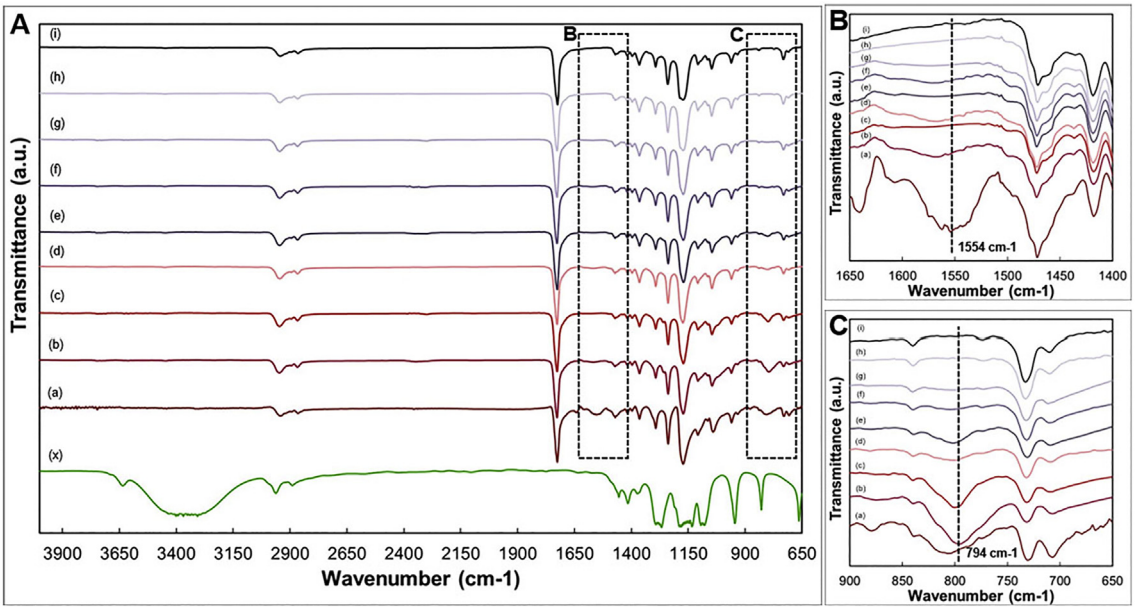

Fig. 2. (**A**) ATR-FTIR spectra for PCL-PANI fibers (**a**) 88:12, (**b**) 91:9, (**c**) 93:7, (**d**) 94:6, (**e**) 95:5, (**f**) 96.25:3.75, (**g**) 97.5:2.5, (**h**) 98.75:1.25. The spectra for the reference materials (**i**) neat PCL 13% fibers and (**x**) PANI:CSA complex are also shown. (**B**) Close caption of the 1400–1650 cm^{-1} region with special focus on the peaks at 1554 cm^{-1}; (**C**) Close caption of the 650–900 cm^{-1} region with special focus on the peaks at 794 cm^{-1}. (resolution 4 cm^{-1}, 32 scans).

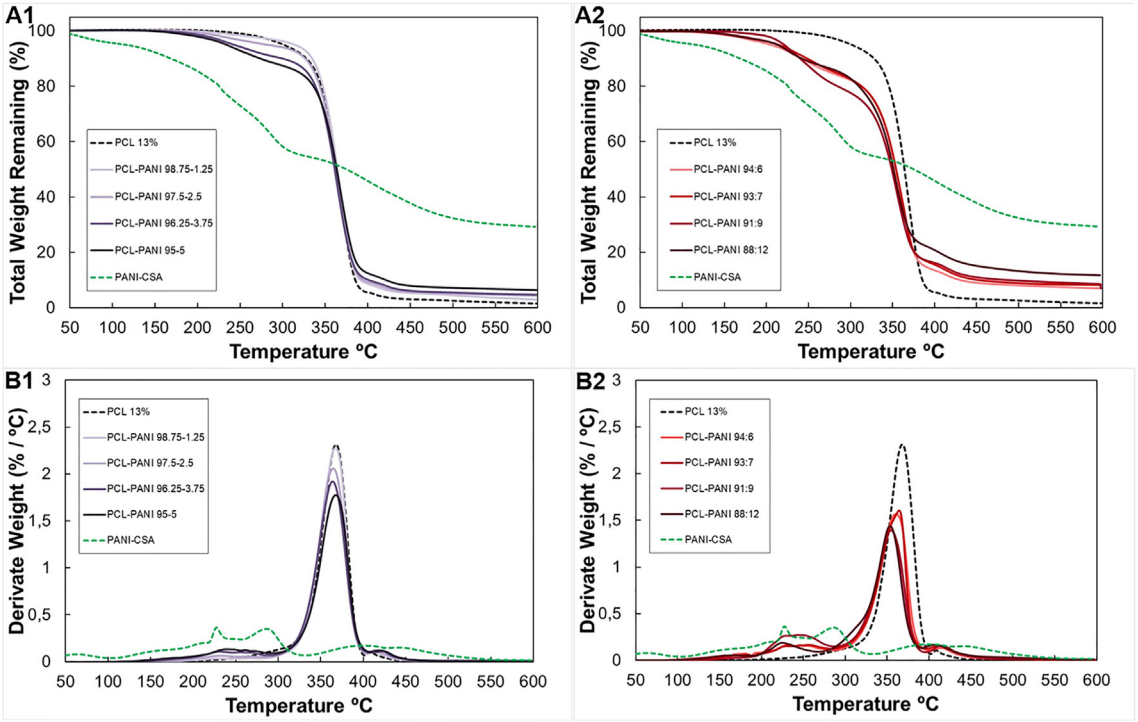

Fig. 3. TGA profiles (**A1** and **A2**) and respective first derivates (**B1** and **B2**), of PCL-PANI electrospun fibers with different PCL to PANI ratios. All samples include profiles for the standards used (neat PCL 13% fibers and PANI-CSA powder) (1.5 °C min^{-1}, 50–600 °C).

PCL and PANI:CSA were identified.

3.3. TGA analysis and calculation of the component's relative amounts

TGA results also showed the incorporation of PANI in the fibers prepared from the blends solutions. Fig. 3 shows the thermograms for the various PCL-PANI fibers, PCL(13%) fibers and for a sample of PANI-CSA. The important data extracted from these curves are shown in Table 2. We observed that the onset of fiber blend degradation occurs at lower temperatures than that of pure PCL fibers. This lower thermal stability is attributed to the presence of PANI-CSA, which has an onset degradation temperature at ~168.1 °C (Fig. 3) that is closer to the initial onset temperature for the blended fibers (189.1 ± 6.7 °C). At this stage the total mass loss increased with increasing amounts of PANI:CSA (Table 2). The second onset temperature for the PCL:PANI fibers occurs at 343.4 ± 6.3 °C, close to the onset of neat PCL fibers degradation at 341.6 °C. This second onset temperature remained stable in all the samples tested, and the relative amount of mass loss at this stage also decreased with the increasing fiber content of PANI:CSA. The amount of lost material roughly corresponds to the PCL present in the PCL-PANI fibers, since PANI:CSA loss started at 303.5 °C, and was broad enough to overlap with the PCL onset temperature. A third onset temperature was observed at 437.8 ± 5.2 °C in all the PCL-PANI fibers, also present on PCL fibers (427.0 °C). This loss corresponds to PCL degradation and correlates to total mass loss of the fibers and the PANI:CSA content. The amount of residue at 600 °C also increased with the increasing amount of PANI:CSA in the fibers, probably due to remaining PANI degradation products. Overall, from these data we can conclude that all the PCL-PANI samples are different, with onset temperatures overlapping with ones from PCL and PANI:CSA standard.

3.4. Electroconductivity

PANI:CSA incorporation into the fibers resulted in electroconductive fiber mats (Fig. 4). Higher PANI:CSA content was associated with higher conductivity values, reaching a maximum of 7.7×10^{-2} S cm^{-1} for PCL-PANI (88:12), 4.2×10^{-2} S cm^{-1} for PCL-PANI (95:5) and 3.4×10^{-2} S cm^{-1} for PCL-PANI (93:7). The remaining samples showed decreased conductivity: 96.25:3.75 > 91:1 > 94:6 > 97.5:2.5 > 98.75:1.25. The increase of the fiber electroconductivity was proportional to PANI:CSA content in the fibers up to PCL-PANI 95:5 and a plateau was reached until PCL-

Table 2
TGA data compilation for the tested fibers (1.5 °C per min, 50–600 °C), including onset temperature for material degradation (°C) and corresponding weight loss (w/w %). Tn = Temperature onset n, n = 1, 2, 3.

Sample	Onset T1 (°C)	Peak T1 (°C)	Weight Loss T1 (%)	Onset T2 (°C)	Peak T2 (°C)	Weight Loss T2 (%)	Onset T3 (°C)	Peak T3 (°C)	Weight Loss T3 (%)	Residue (%)
88:12	187.3	225.0	12.8	329.7	359.4	64.8	367.4	411.1	10.7	11.7
91:9	195.7	230.7	20.4	355.6	349.8	62.6	358.2	408.6	8.1	8.9
93:7	190.4	256.7	14.9	337.5	364.3	68.2	380.2	412.1	8.0	8.9
94:6	182.1	231.4	16.1	336.6	360.4	70.0	380.7	414.3	6.7	7.2
95:5	196.3	237.2	12.0	344.9	367.8	76.5	388.3	418.49	5.4	6.2
96.25:3.75	195.5	229.7	9.3	342.0	364.0	81.5	395.6	421.6	4.6	4.5
97.5:2.5	186.9	230.4	5.3	342.3	364.7	85.9	389.6	413.3	4.6	4.2
98.75:1.25	178.2	267.7	2.8	344.9	367.4	89.2	387.24	412.4	5.3	2.7
PCL 13%	–	–	–	341.6	368.0	94.6	387.6	408.6	3.9	1.5

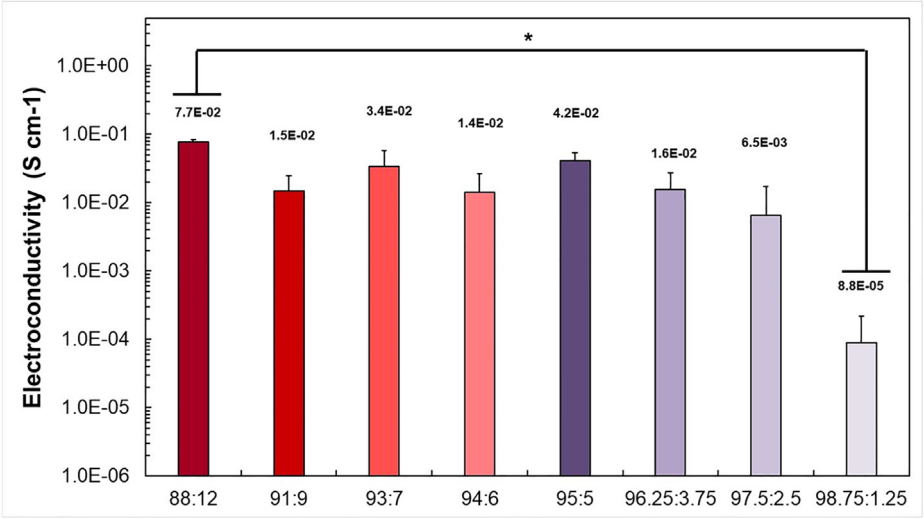

Fig. 4. Electroconductivity values for the PCL-PANI blends tested. All samples were statistically compared against PCL-PANI 98.75:1.25 (* = $p < 0.05$). Results are presented as mean ± sd (n = 3).

PANI 88:12.

The results obtained indicate that the minimum PCL:PANI ratio necessary to turn PCL fibers conductive is 96.25:3.75. However, only sample 88:12 was statistically different from the least conductive sample 98.75:1.25 (8.8×10^{-5} S cm^{-1}).

3.5. Mechanical properties

The addition of PANI:CSA to PCL altered the properties of the fiber mat. Maximum extension significantly decreased for all the samples tested (Figs. 5 **and S3**). They were all more fragile and brittle. Interestingly, Young's modulus only increased for samples 96.25:3.75, 97.5:2.5 and 98.75:1.25 when compared with PCL 13% fibers.

When comparing only samples 98.75:1.25, 97.5:2.5, 96.25:3.75, and 95:5 addition of PANI:CSA is correlated with a decrease in the Young's tensile modulus, UTS and Maximum extension (Fig. 5). For samples 94:6, 93:7, 91:9 and 88:12 similar trends were observed. Statistically significant differences were observed only among these 2 groups, where decreasing PCL content influenced only Young's tensile modulus.

3.6. Cell viability and kinetic data

ReN-VM cells (Passage 10) were grown on the fibers after standard poly-ornithine and laminin coating. An equivalent number of cells (Fig. 6), calculated from reduced Alamar Blue was determined at days 1, 3, 5, and 7. Cell adhesion, doubling time, and growth rate (Table 3) were calculated from these values.

High amounts of PANI:CSA are associated with a lower cell adhesion at day 1, roughly less 50% when compared to the pristine PCL

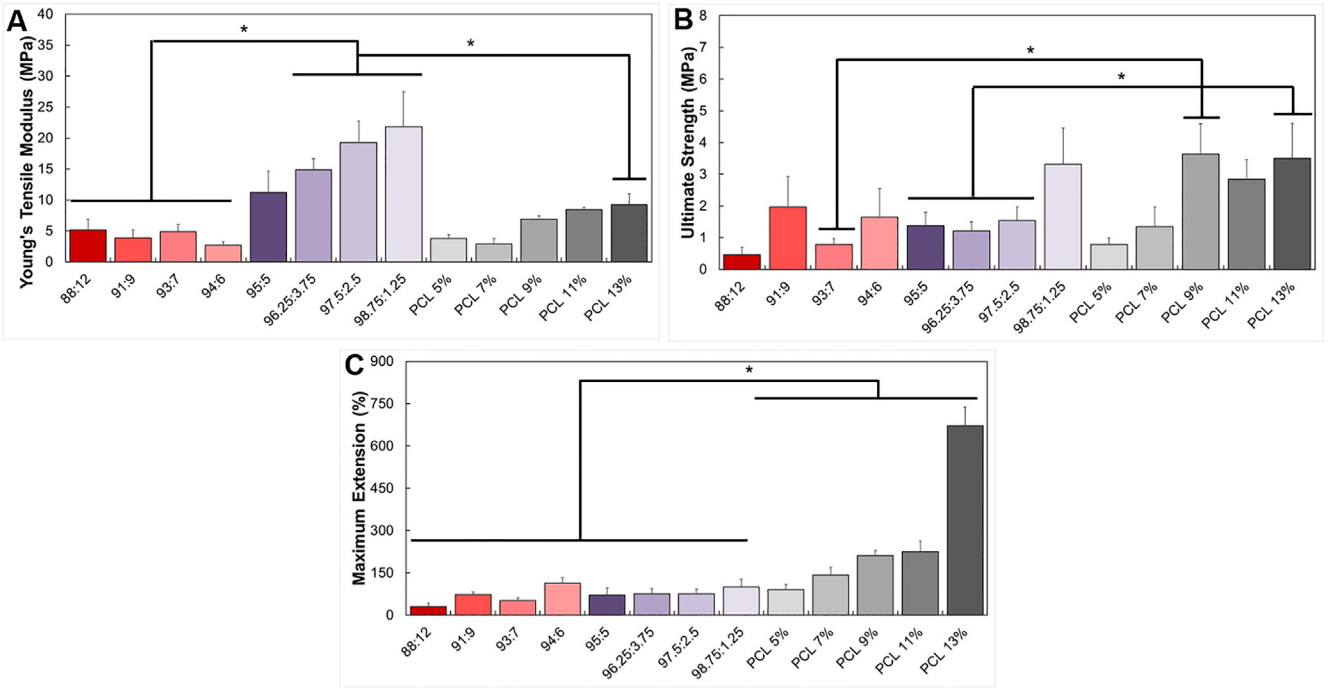

Fig. 5. Mechanical properties of the tested PCL-PANI fibers and respective PCL control standard fibers: (**A**) Young's tensile modulus, (**B**) Ultimate strength and (**C**) Maximum extension. Respective PCL fibers (5% to 13%) were used as controls (* means $p < 0.05$).

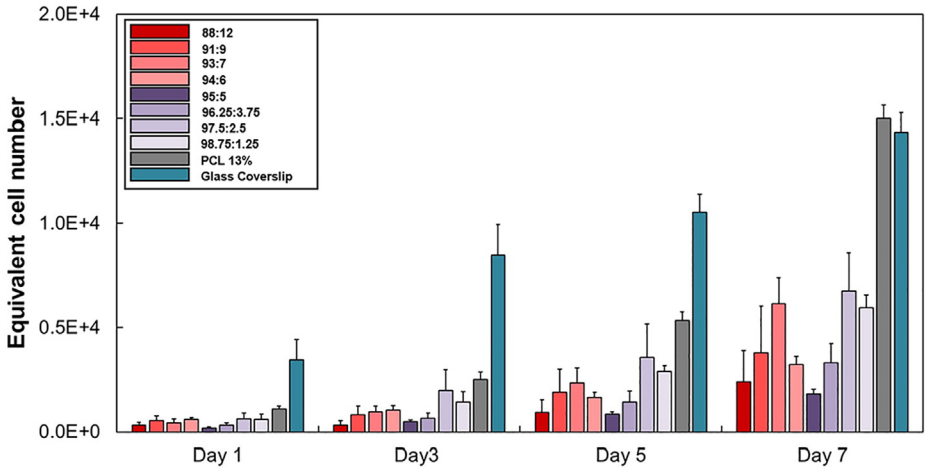

Fig. 6. Cell growth profile at days 1, 3, 5, and 7 using the equivalent number of cells (mean + std, n = 3). Glass coverslips and PCL 9% fibers were used as controls.

Table 3
Cell kinetics data obtained from the growth curve data. Growth rate and doubling time were calculated between days 3 and 7.

Sample	Adhesion (%)	Growth Rate (per day)	Doubling time (h^{-1})
88:12	9	0.50	33
91:9	14	0.38	44
93:7	11	0.46	36
94:6	16	0.28	59
95:5	5	0.34	49
96.25:3.75	9	0.41	41
97.5:2.5	17	0.31	54
98.75:1.25	16	0.36	47
PCL 13%	29	0.45	37
Glass Coverslip	92	0.13	126

fibers (Tables 3 **and S2**). This suggests that PANI:CSA incorporation decreased cell retention on the fiber mats. However, the absolute number of cells adhered to the electrospun matrix were sufficient to further investigate the cell-cell interactions. From a research point of view, the low initial cell density allows one to follow the scaffold colonization and cell visualization more efficiently. The low initial adhesion efficiency might eventually be improved by either optimization of the seeding protocol and/or incorporation of adhesion molecules that do not compromise fiber electroconductivity. Growth rate was higher on PCL-PANI fibers with higher PANI:CSA content, especially when compared to the corresponding PCL fibers.

Despite low adhesion values, both Alamar Blue (Fig. 6), DAPI/Phalloidin staining and SEM imaging (Figs. 7 **and S4**) demonstrate the presence of adherent and viable cells growing on the fiber mats throughout the entire experiment.

DAPI-phalloidin and SEM images show that cells growing on PCL-PANI fibers are further apart than on PCL fibers (Fig. 7). This effect is negated when PANI:CSA content decreased below a certain value (sample 97. 5:2.5), from where cells form clusters more frequently. One interesting feature observed in these images is cells growing on PCL-PANI (Fig. 7) and PCL fibers (**Fig. S4**) maintain their normal spindle-shaped/stellar morphology, stretching along the fiber mat with no apparent orientation. These results suggest that PCL-PANI fibers are biocompatible in terms of both cell adhesion and growth and allow NSCs to retain their natural morphology.

4. Discussion

Previous studies have shown the potential of PANI-PCL blended fibers as gas sensors [32] or as scaffolds for culturing myoblasts and HUVECs, [33,34] suggesting that this blend might be a suitable candidate for neural cell culture. Based on this, we hypothesized that a biocompatible and electroconductive scaffold for neural tissue engineering might be obtained by blending these two polymers. The goal of this study is to optimize this blend and characterize the resulting NSC-compatible and electrically conductive PCL-PANI electrospun scaffolds. Achieving this goal will lead to a biocompatible in vitro platform for drug screening and disease modelling. Such platform can also serve as an interface for deep-brain electrodes or allow the direct transplantation of fully grown and functional neurons into patients' brains.

Understanding how the fiber diameter varies is helpful in determining how suitable the non-woven fibermats are as matrices for neural regeneration. All the fibers obtained have diameters within the nanoscale range (< 350 nm) and afford uniform fibermats, which according to the literature should facilitate NSC proliferation by promoting cell migration and reducing the effect of topographic cues that otherwise would lead to neural cell differentiation [36]. Blended fiber samples of 95:5, 94:6, 93:7, however, have similar diameters, and in samples 91:1 and 88:12 the drop observed for fiber is significant. There were no statistically significant differences between sample 95:5 and samples 94:6 and 93:7, or between samples 96.25:3.75, 97.50:2.50 and 98.75:1.25. However, increasing PANI:CSA content reduced the standard deviation of the average fiber diameter. This might be the result of a greater charge distribution through the fibers during electrospinning, caused by increasing amounts of PANI:CSA. This makes the solvent evaporation rate more uniform and promotes the production of a more homogeneous population of fibers.

TGA and FTIR data confirms the presence of all components in the fibers. TGA shows that they are also in the right proportions and degrade in a predictable way, while FTIR also proves that no interactions are visible between PCL and PANI:CSA.

The FTIR of the PANI:CSA standard does not show a PANI shoulder band from 1650 to 4000 cm^{-1}, suggesting that CSA doping successfully affords a conductive form of PANI:CSA [37]. The doping used in this project, 0.78 g of PANI for 1 g of CSA, is similar to the optimal literature values, affording doping of 50% of amine groups in the polymer chain and giving the maximum electroconductivity possible. Values below or above 50–60% doping are known to reduce polymer's conductivity [23,37,38].

An early onset temperature in TGA correlates with the presence of PANI:CSA mixture in the fibers, and higher contents are associated with bigger steps in the curve. The presence of separate and constant onset temperatures in the TGA profiles and the absence of visible changes on FTIR's peak intensities indicates that these two polymers do not mix when blended together in the fibers. This conclusion is supported also by the DSC results (**Fig. S2**). No major changes in the Tg values of PCL

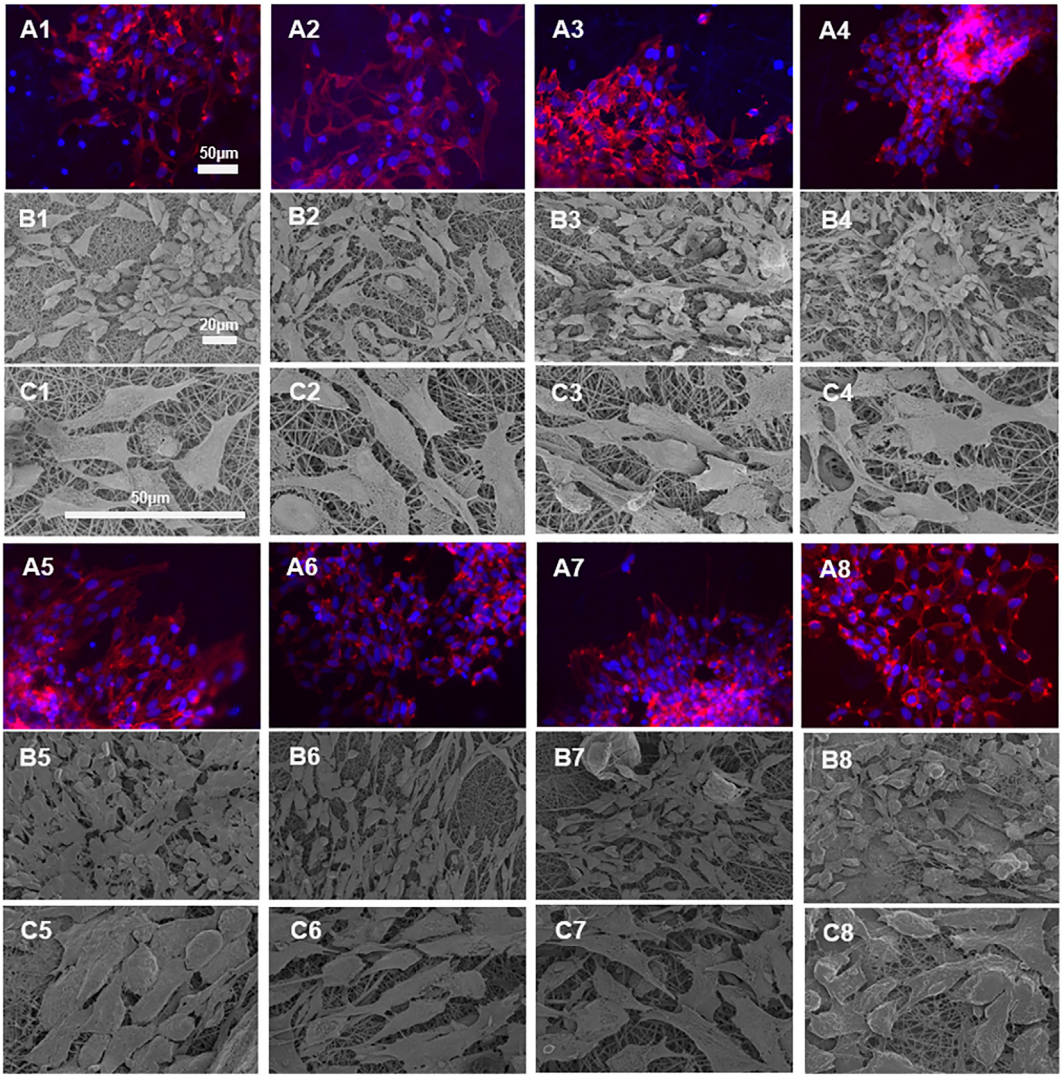

Fig. 7. DAPI/Phalloidin (**A** 400X scale bar 50 μm) and SEM images (**B** 2000X scale bar 20 μm, **C** 5000X scale bar 50 μm) of ReN-VM cells growing on PCL-PANI fibers after 10 days in culture. PCL-PANI fibers tested: (**A1, B1, C1**) 95:5, (**A2, B2, C2**) 96.25:3.75, (**A3, B3, C3**) 97.5:2.5, (**A4, B4, C4**) 98.75:1.25, (**A5, B5, C5**) 94:6, (**A6, B6, C6**) 93:7, (**A7, B7, C7**) 91:9, (**A8, B8, C8**) 88:12.

were observed in any of the samples tested by DSC, and Tm doesn't vary significantly among all the samples tested. This proves that there is phase separation between the components when they are together in a blend fiber (**Fig. S3**) [39]. In fact, higher PANI:CSA amounts decreases the energy released by the system when crystallization occurs (88:12, 91:9, 93:7, 94:6) (**Table S1**), confirming that the interactions formed are not stable and supporting the previously observed increasing fragility of the fibers with PANI:CSA content. These features hadn't any effect on the electrospinnability of the tested solutions, since the process was stable and homogeneous mats were obtained.

Because the stabilizing forces involved aren't strong, increasing amounts of PANI:CSA disrupt the interactions and make the fibers progressively softer and more fragile. In fact, the Young's tensile modulus is low for fibers having high amounts of PANI:CSA. However, approaching the native modulus value of brain tissue (7.11–9.21 KPa) is an important designing feature for neural tissue scaffolds, since it promotes not only its biocompatibility but also efficient cell differentiation [40–43].

In this study, samples with PCL-PANI ratio above 95:5 showed high electroconductivity values, namely samples 88:12, 95:5 and 93:7 (7.7×10^{-2} S/cm, 4.2×10^{-2} S/cm and 3.4×10^{-2} S/cm respectively). These values are lower than the ones described for polyaniline films (2.7×10^{2} S/cm) [23], but are in line with the one Low and coworkers obtained for their PCL-PANI fibers used for gas sensing (8.0×10^{-2} S/cm) [32]. Interestingly, most of the fibers tested surpass the conductivity of biological fluids ($\sim 1 \times 10^{-2}$ S/cm), suggesting that these fiber mats are suitable candidates for further studies.

The existence of a plateau phase between samples 95:5 and 88:12 is not easily explained, since electroconductivity should have increased proportionally to PANI content. Increased concentrations of PANI can lead to the formation of capacitors, impacting current passing as was reported before [39,44]. Because these fibers were made with much higher concentrations, it is possible that capacitor formation might explain the plateau phase observed in electroconductivity.

In this work, 1,1,1-Trifluoroethanol is used as the solvent for the PCL-PANI solutions produced. The solubility of PANI in TFE is similar to that in 1,1,1,3,3,3-hexafluoropropan-2-ol (HFP) [45]. HFP can actually enhance PANI:CSA electroconductivity by acting as a pseudo dopant and stabilizing its resonance structure through hydrogen bridges between the alcohol group of HFP and imine groups of PANI:CSA, promoting PANI:CSA chain uncoiling and relaxation by blocking chain-chain interactions through its bulky fluoride groups [46]. TFE should show a similar mechanism for chain relaxation and electroconductivity enhancement for fibers [45]. Since the fibers obtained are also

electroconductive, TFE can therefore be viewed as a more economical alternative to HFP. However, care must be taken with TFE since high humidity values (40–50%) during electrospinning can negatively affect the conductivity of the samples tested.

Both PCL and PANI:CSA are generally viewed as biocompatible materials [27,47,48]. Another goal in this study is also to confirm that these mats can be used in NSC culture. Since cells were able to adhere, the cell growth values obtained were high for all PCL-PANI fibermats and the cells maintained a normal spindle-shaped/stellar morphology we conclude that PANI:CSA have minimal toxic effects when incorporated into PCL for NSCs.

In the fabricated fiber mats, increased amounts of PANI:CSA in the fibers were associated with a lower adhesion at day 1, possibly the result of PANI:CSA decreasing the contact angle of the fibers [49]. However, this did not compromise their interaction with the electrospun fibers, as it is shown in the SEM images where the cells are intimately interacting with the fiber mats.

Due to the low adhesion observed, the initial cell number was low for all the PCL-PANI samples. However, the cell growth rate on all the samples tested containing PANI:CSA is similar to neat PCL fibers (Tables 3 **and S2**). When analyzing PCL-PANI samples alone, growth rate tended to be higher with increased PANI:CSA content. Since initial cell adhesion was low for these samples, the cells had more scaffold surface to spread and grow, which is visible in Fig. 7**.** It is hypothesized that this minimized cell-cell contact inhibition of growth and prevented the formation of cell clusters as seen on PCL samples (**Fig. S4**) [36,50].

The doubling time values for cells growing on PCL-PANI fibers were lower and not close to the values described in the literature for ReN-VM cell growth on tissue culture plates (23.8 h).

It was reported in the literature that NSCs growing on electrospun PES fibers with diameters of 283 ± 45 nm show a higher proliferative potential than on similar fibers of larger diameters (749 ± 153 nm and 1452 ± 312 nm), but spread less across the fiber mat and instead form clusters [36]. In our study all the fibers tested (except for PCL 13%), were all closer in size to 283 ± 45 nm. Cluster formation wasn't commonly observed with PCL-PANI fibers and, what is more, the growth rate is higher when compared to the neat PCL fibers tested. This suggests that the effect of fiber diameter is not enough to explain the differences observed.

As a final note, since cell growth is observed and cell's maintain a normal spindle-shaped/stellar morphology we can assume that PANI:CSA has minimal toxic effects when incorporated into PCL for NSCs [25].

5. Conclusions

PCL-PANI nanofibers were obtained and characterized through SEM, FTIR, TGA and DSC. For the first time it was demonstrated that NSCs were able to adhere and grow on these fibers, maintaining both their viability and spindle-shaped/stellar morphology. Thus, the fibers obtained were shown to be biocompatible for NSCs, allowing these fiber mats to potentially be used for neural cell culture. For sample 88:12, the electroconductivity (7.7×10^{-2} S cm^{-1}), the low young's module and good cell kinetic properties justify further cell studies. The fibers obtained still require further optimization to improve their mechanical and cell-adhesive properties, as well as modulation to improve their electroconductivity throughout cell culturing. The development of biocompatible and electroconductive PCL-PANI fibers will facilitate improved studies of neural cell studies, pivotal for obtaining the appropriate cell morphology to either test neuroactive drugs, advance tissue engineering strategies, or use for indirect therapies such as deep brain stimulation, key for treating neurodegenerative diseases.

Acknowledgements

All authors thank the support from the Center for Biotechnology & Interdisciplinary Studies (CBIS), as well as of the following CBIS cores for all the analysis made: Analytical Biochemistry (Joel Morgan, PhD), Microscopy Research (Sergey Pryshchep, PhD) and Nanoscale characterization (Deniz Rende, PhD). The authors also thank the assistance from all the personal from MNCR-cMDIS-RPI cleanroom facility for SEM (Mr. David Frey, BSc) and 4-proble analysis (Bryant Colwill, BSc; Sarah An, PhD; John Barthel, BSc).

F.F.F. Garrudo and J.C. Silva gratefully acknowledge the support the financial support from FCT through the scholarships PD/BD/114045/2015 and SFRH/BD/105771/2014 respectively.

Funding received by iBB - Institute for Bioengineering and Biosciences from FCT - Portuguese Funding for Science and Technology (UID/BIO/04565/2013) and from Programa Operacional Regional (POR) de Lisboa 2020 (Project N. 007317) is acknowledged. We also acknowledge the funding received from POR de Lisboa 2020 through the project PRECISE - Accelerating progress toward the new era of precision medicine (Project N. 16394) and to FCT through the project NEURON, PTDC/CTM-CTM/30237/2017. F. Garrudo and J Silva acknowledges FCT for the PhD fellowships PD/BD/114045/2015 and PD/BD/105771/2014, respectively.

Appendix A. Supplementary material

Supplementary data to this article can be found online at https://doi.org/10.1016/j.eurpolymj.2019.04.048.

References

[1] M. Erkkinen, M.-O. Kim, M. Geschwind, Clinical neurology and epidemiology of the major neurodegenerative diseases, Csh Persp. Biol. 10 (2018) a033118.
[2] C.-C. Wu, C.-C. Lien, W.-H. Hou, P.-M. Chiang, K.-J. Tsai, Gain of BDNF function in engrafted neural stem cells promotes the therapeutic potential for Alzheimer's disease, Scient. Rep. 6 (2016) 27358.
[3] N. Payne, A. Sylvain, C. O'Brien, D. Herszfeld, S.G. biotechnology, Application of human induced pluripotent stem cells for modeling and treating neurodegenerative diseases, New Biotechnol. 32 (2015) 212–228.
[4] Y. Wang, X. Ji, R. Leak, F. Chen, G. Cao, Stem cell therapies in age-related neurodegenerative diseases and stroke, Age. Res. Rev. 34 (2017) 39–50.
[5] D. Carradori, J. Eyer, P. Saulnier, V. Préat, A. des Rieux, The therapeutic contribution of nanomedicine to treat neurodegenerative diseases via neural stem cell differentiation, Biomaterials 123 (2017) 77–91.
[6] S. Marsh, M. Blurton-Jones, Neural stem cell therapy for neurodegenerative disorders: the role of neurotrophic support, Neurochem. Int. 106 (2017) 94–100.
[7] A. Trounson, C. McDonald, Stem cell therapies in clinical trials: progress and challenges, Cell Stem Cell 17 (2015) 11–22.
[8] A. Khademhosseini, R. Langer, A decade of progress in tissue engineering, Nat. Protocols 11 (2016) 1775.
[9] K. Yang, S. Yu, J. Lee, H.-R. Lee, G.-E. Chang, J. Seo, et al., Electroconductive nanoscale topography for enhanced neuronal differentiation and electrophysiological maturation of human neural stem cells, Nanoscale 9 (2017) 18737–18752.
[10] H. Wang, M. Mullins, J. Cregg, C. McCarthy, R. Gilbert, Varying the diameter of aligned electrospun fibers alters neurite outgrowth and Schwann cell migration, Acta Biomater. 6 (2010) 2970–2978.
[11] W. Zhu, T. Ye, S.-J. Lee, H. Cui, S. Miao, X. Zhou, et al., Enhanced neural stem cell functions in conductive annealed carbon nanofibrous scaffolds with electrical stimulation, nanomedicine: nanotechnology, Biol. Med. 14 (2017) 2485–2494.
[12] F. Pires, Q. Ferreira, C. Rodrigues, J. Morgado, F. Ferreira, Neural stem cell differentiation by electrical stimulation using a cross-linked PEDOT substrate: expanding the use of biocompatible conjugated conductive polymers for neural tissue engineering, Biochim. et Biophys. Acta (BBA) – General Sub. 1850 (2015) 1158–1168.
[13] M. Dodel, N. Nejad, S. Bahrami, M. Soleimani, L. Amirabad, H. Hanaee-Ahvaz, et al., Electrical stimulation of somatic human stem cells mediated by composite containing conductive nanofibers for ligament regeneration, Biologicals 46 (2017) 99–107.
[14] J. Zhang, K. Qiu, B. Sun, J. Fang, K. Zhang, H. EI-Hamshary, et al., The aligned core–sheath nanofibers with electrical conductivity for neural tissue engineering, J. Mater. Chem. B 2 (2014) 7945–7954.
[15] M. Adel, M. Zahmatkeshan, B. Johari, S. Kharrazi, M. Mehdizadeh, B. Bolouri, et al., Investigating the effects of electrical stimulation via gold nanoparticles on in vitro neurite outgrowth: Perspective to nerve regeneration, Microelectron. Eng. 173 (2017) 1–5.
[16] N. Suthana, Z. Haneef, J. Stern, R. Mukamel, E. Behnke, B. Knowlton, et al., Memory enhancement and deep-brain stimulation of the entorhinal area, New England J. Med. 366 (2012) 502–510.
[17] J. Jacobs, J. Miller, S. Lee, T. Coffey, A. Watrous, M. Sperling, et al., Direct electrical stimulation of the human entorhinal region and hippocampus impairs memory,

Neuron 92 (2016) 983–990.
[18] Y. Ezzyat, J. Kragel, J. Burke, D. Levy, A. Lyalenko, P. Wanda, et al., Direct brain stimulation modulates encoding states and memory performance in humans, Curr. Biol. 27 (2017) 1251–1258.
[19] T. Qazi, R. Rai, D. Dippold, J. Roether, D. Schubert, E. Rosellini, et al., Development and characterization of novel electrically conductive PANI–PGS composites for cardiac tissue engineering applications, Acta Biomater. 10 (2014) 2434–2445.
[20] J. Shin, E. Choi, J. Cho, A.-N. Cho, Y. Jin, K. Yang, et al., Three-dimensional electroconductive hyaluronic acid hydrogels incorporated with carbon nanotubes and polypyrrole by catechol-mediated dispersion enhance neurogenesis of human neural stem cells, Biomacromolecules 18 (2017) 3060–3072.
[21] R. Balint, N. Cassidy, S. Cartmell, Conductive polymers: towards a smart biomaterial for tissue engineering, Acta Biomater. 10 (2014) 2341–2353.
[22] P. Sensharma, G. Madhumathi, R.D. Jayant, A.K. Jaiswal, Biomaterials and cells for neural tissue engineering: current choices, Mater. Sci. Eng. C 77 (2017) 1302–1315.
[23] E.R. Holland, S.J. Pomfret, P.N. Adams, A.P. Monkman, Conductivity studies of polyaniline doped with CSA, J. Phys.: Condens. Matt. 8 (1996) 2991–3002.
[24] M. Li, Y. Guo, Y. Wei, A. MacDiarmid, P. Lelkes, Electrospinning polyaniline-contained gelatin nanofibers for tissue engineering applications, Biomaterials 27 (2006) 2705–2715.
[25] L. Ghasemi-Mobarakeh, M.P. Prabhakaran, M. Morshed, M.H. Nasr-Esfahani, S. Ramakrishna, Electrical stimulation of nerve cells using conductive nanofibrous scaffolds for nerve tissue engineering, Tissue Eng. Part A 15 (2009) 3605–3619.
[26] E. Yslas, P. Cavallo, D. Acevedo, C. Barbero, V. Rivarola, Cysteine modified polyaniline films improve biocompatibility for two cell lines, Mater. Sci. Eng.: C 51 (2015) 51–56.
[27] P. Humpolíček, V. Kašpárková, J. Pacherník, J. Stejskal, P. Bober, Z. Capáková, et al., The biocompatibility of polyaniline and polypyrrole: a comparative study of their cytotoxicity, embryotoxicity and impurity profile, Mater. Sci. Eng.: C 91 (2018) 303–310.
[28] G. Thrivikraman, G. Madras, B. Basu, Intermittent electrical stimuli for guidance of human mesenchymal stem cell lineage commitment towards neural-like cells on electroconductive substrates, Biomaterials 35 (2014) 6219–6235.
[29] S. Bhang, S. Jeong, T. Lee, I. Jun, Y. Lee, B. Kim, et al., Electroactive electrospun polyaniline/poly [(l lactide)co (caprolactone)] fibers for control of neural cell function, Macromole. Biosci. 12 (2012) 402–411.
[30] D. Mawad, E. Stewart, D. Officer, T. Romeo, P. Wagner, K. Wagner, et al., A single component conducting polymer hydrogel as a scaffold for tissue engineering, Adv. Funct. Mater. 22 (2012) 2692–2699.
[31] V. Guarino, M. Alvarez-Perez, A. Borriello, T. Napolitano, L. Ambrosio, Conductive PANi/PEGDA macroporous hydrogels for nerve regeneration, Adv. Healthc. Mater. 2 (2013) 218–227.
[32] K. Low, N. Chartuprayoon, C. Echeverria, C. Li, W. Bosze, N. Myung, et al., Polyaniline/poly(ε-caprolactone) composite electrospun nanofiber-based gas sensors: optimization of sensing properties by dopants and doping concentration, Nanotechnology 25 (2014) 115501.
[33] S. Ku, S. Lee, C. Park, Synergic effects of nanofiber alignment and electroactivity on myoblast differentiation, Biomaterials 33 (2012) 6098–6104.
[34] Y. Li, X. Li, R. Zhao, C. Wang, F. Qiu, B. Sun, et al., Enhanced adhesion and proliferation of human umbilical vein endothelial cells on conductive PANI-PCL fiber scaffold by electrical stimulation, Mater. Sci. Eng. C 72 (2017) 106–112.
[35] S.-Y. Ng, G. Bogu, B. Soh, L. Stanton, The long noncoding RNA RMST interacts with SOX2 to regulate neurogenesis, Mole. Cell 51 (2013) 349–359.
[36] G. Christopherson, H. Song, H.-Q. Mao, The influence of fiber diameter of electrospun substrates on neural stem cell differentiation and proliferation, Biomaterials 30 (2009) 556–564.
[37] N. Blinova, J. Stejskal, M. Trchová, J. Prokeš, Control of polyaniline conductivity and contact angles by partial protonation, Polym. Int. 57 (2008) 66–69.
[38] W. Focke, G. Wnek, Conduction mechanisms in polyaniline (emeraldine salt), J. Electroanal. Chem. Interf. Electrochem. 256 (1988) 343–352.
[39] R. Basheer, A. Hopkins, P. Rasmussen, Dependence of transition temperatures and enthalpies of fusion and crystallization on composition in polyaniline/nylon blends, Macromolecules 32 (1999) 4706–4712.
[40] K. Miller, K. Chinzei, Mechanical properties of brain tissue in tension, J. Biomech. 35 (2002) 483–490.
[41] A. Engler, S. Sen, H. Sweeney, D. Discher, Matrix elasticity directs stem cell lineage specification, Cell 126 (2006) 677–689.
[42] M. Nogueira, O. Lafitte, J.-M. Steyaert, H. Bakardjian, B. Dubois, H. Hampel, et al., Mechanical stress related to brain atrophy in Alzheimer's disease, Alzheimer's Dementia 12 (2016) 11–20.
[43] S. Ali, I. Wall, C. Mason, A. Pelling, F. Veraitch, The effect of Young's modulus on the neuronal differentiation of mouse embryonic stem cells, Acta Biomater. 25 (2015) 253–267.
[44] R. Chernozem, M. Surmeneva, R. Surmenev, Hybrid biodegradable scaffolds of piezoelectric polyhydroxybutyrate and conductive polyaniline: piezocharge constants and electric potential study, Mater. Lett. 220 (2018) 257–260.
[45] Y. Cao, J. Qiu, P. Smith, Effect of solvents and co-solvents on the processibility of polyaniline: I solubility and conductivity studies, Synth. Metals 69 (1995) 187–190.
[46] A.R. Hopkins, P.G. Rasmussen, Characterization of solution and solid state properties of undoped and doped polyanilines processed from hexafluoro-2-propanol, Macromolecules 29 (1996) 7838–7846.
[47] P. Humpolicek, V. Kasparkova, P. Saha, J. Stejskal, Biocompatibility of polyaniline, Synth. Metals 162 (2012) 722–727.
[48] Radaszkiewicz Humpolíček, Stejskal Kašpárková, Kuceková Trchová, et al., Stem cell differentiation on conducting polyaniline, Rsc Adv. 5 (2015) 68796–68805.
[49] Y. Arima, H. Iwata, Effect of wettability and surface functional groups on protein adsorption and cell adhesion using well-defined mixed self-assembled monolayers, Biomaterials 28 (2007) 3074–3082.
[50] M. Leino, C. Astrand, N. Hughes-Brittain, B. Robb, R. McKean, V. Chotteau, Human embryonic stem cell dispersion in electrospun PCL fiber scaffolds by coating with laminin-521 and E-cadherin-Fc, J. Biomed. Mater. Res. Part B: Appl. Biomater. 106B (2017) 1226–1236.